YuZhang Bi · YanJun Du · SiMing He · XinPo Sun · DongPo Wang · XinPo Li · Heng Liang · Yong Wu

Numerical analysis of effect of baffle configuration on impact force exerted from rock avalanches

Abstract In mountainous areas, channelized rock avalanches swarm downslope leading to large impact forces on building structures in residential areas. Arrays of rock avalanche baffles are usually installed in front of rigid barriers to attenuate the flow energy of rock avalanches. However, previous studies have not sufficiently addressed the mechanisms of interaction between the rock avalanches and baffles. In addition, empirical design approaches such as debris flow (Tang et al., Quat Int 250:63–73, 2012), rockfall (Spang and Rautenstrauch, 1237–1243, 1988), snow avalanches (Favier et al., 14:3–15, 2012), and rock avalanches (Manzella and Labiouse, Landslides 10:23–36, 2013), which are applied in natural geo-disasters mitigation cannot met construction requirements. This study presents details of numerical modeling using the discrete element method (DEM) to investigate the effect of the configuration of baffles (number and spacing of baffle columns and rows) on the impact force that rock avalanches exert on baffles. The numerical modeling is firstly conducted to provide insights into the flow interaction between rock avalanches and an array of baffles. Then, a modeling analysis is made to investigate the change pattern of the impact force with respect to baffle configurations. The results demonstrate that three crucial influencing factors (baffle row numbers, baffle column spacing, and baffle row spacing) have close relationship with energy dissipation of baffles. Interestingly, it is found that capacity of energy dissipation of baffles increases with increasing baffle row numbers and baffle row spacing, while it decreases with increasing baffle column spacing. The results obtained from this study are useful for facilitating design of baffles against rock avalanches.

Keywords Rock avalanches · Discrete element method · Baffles · Interaction mechanisms · Energy dissipation

Introduction

Rock avalanche means extremely rapid, massive, flow-like motion of fragmented rock from a large rock slide or rockfall (Hungr et al. 2014), which is known to be one of the most dangerous landslide processes with high destructive impact energy, commonly occurs in southwest China (Xu et al. 2009; Zhang et al. 2015; Xing et al. 2015; Bi et al. 2016a; Li et al. 2016). Previous studies (Cruden et al. 1990) suggest that "rock avalanches" should be reserved for events exceeding about 1 million m³. However, the definition nowadays is quite different in comparison to its early beginnings. Some very mobile, small rock avalanches have been described by Hungr et al. (2014), Hutchinson (2002), Bi et al. (2016a), and Zhan et al. (2017). What is more, 38 rock avalanches with volumes ranging from 0.4 to 50×10^6 m³ in China have been listed by Zhan et al. (2017), which are far less than volume of 1 million m³.

This kind of disasters can be deadly as they can be extremely rapid and may occur without any warning (Bobrowsky and Highland 2013), which bring tremendous damage to residential areas. Countermeasures have been made to minimize the rock avalanche's risk to downstream residential areas or transportation routes (Bugnion et al. 2012; Bi et al. 2016a). There are mainly two kinds of protection structures (Jiang and Towhata 2013; Bi et al. 2016b) that used to minimize this hazard: active ones (e.g., nets) and passive ones (e.g., protection galleries). As active ones is hard to carry out because of avalanches' potential source area is difficult to figure out, engineers and researchers usually choose the passive ones such as flexible barriers, protection galleries, slit dams, and the array baffles (Hauksson et al. 2007; Mancarella and Hungr 2010; Ng et al. 2014; Bi et al. 2016a). Arrays of baffles are usually used as energy dissipaters for avalanches, positioned in the downstream of flow route, mostly in front of the protection zone (Choi et al. 2014a; Law et al. 2015). It is an efficient means to consume the kinetic energy. Experiments have demonstrated that it could slow down the flow via its multi-rows by breaking the flow pattern ibid (Ng et al. 2015): a single row of baffles is ineffective in reducing frontal hazards velocity; however, increasing the array to three rows leads to 65% reduction in runout and up to 57% reduction in frontal velocity.

Studies have been made on the interaction of mechanisms between the debris and rigid barriers (such as retaining wall) (Calvetti et al. 2016). Research has also shown that semi-rigid protection barriers are efficient to defend the rockfall hazard in Alps areas (de Miranda et al. 2015). Hauksson et al. (2007) conducted a series of laboratory experiments with granular material in order to reveal some kinetic relationships between snow avalanches and single mast-like obstacle. Bi et al. (2016b) conducted a series of numerical experiments to reveal the regulations between the rock avalanches' impact force and single defending structure. Thus, the research results can serve as a significant reference for practice engineering using the arrays of baffles. Yet, the interaction mechanisms only reflect the relationships between the geo-disasters and a single obstacle.

Comparing to other protection methods, the arrays of baffle approach has its unique edge in terms of its low construction cost and strong constructability in complex areas, such as steep natural terrain, etc. As this method has potential for use in hazard protection (avalanche protection, debris flow protection, and rockfall protection), many scholars have focused their researches on the arrays of baffles. Ng et al. (2014) implemented laboratory experiments to study the interaction mechanisms between debris flows and mudflow-resistant baffle structures, and quantified the effect of baffle configurations on the increase of flow impedance, which can be taken as an index to evaluate the energy dissipation. Choi et al. (2014b) also conducted a series of numerical experiments to investigate the mechanisms between baffle configuration and impedance of channelized debris flow, yet the scales of experiments are too narrow to reflect the whole picture.

Considering the extent of the number of studies related to baffles energy dissipation, one question that has arisen consistently concerns the impact force that hazards exerted on building structures. Does the impact force have the relationships with the baffles' configuration? What mechanics do they follow between the hazards' impact force, baffles, and structures? This confusion may not only be limited to the general researchers and engineers but also to all the residents which may settle in the potential disaster areas. In the present study, numerical analysis using the three-dimensional Discrete Element Modeling (DEM) is used. DEM is an effective method for studying geological hazards such as rockfall, rock avalanches, debris flow, snow avalanches, and so on. Some theories such as depth-averaged continuum models (Savage 1984; Hungr 1995), smoothed particle hydrodynamics (SPH) (Liang et al. 2017; Dai et al. 2017), lattice Boltzmann method (LBM) (Leonardi et al. 2016), arbitrary Lagrangian-Eulerian finite element method (ALE-FEM) (Kwan et al. 2015), and material point method (MPM) (Li et al. 2016), etc. also apply to the study of geological hazards—even the interaction between hazards and protective structures. However, the methods above-mentioned cannot simulate the whole failure and kinetic process such as the whole block break into individual particles or the effects of segregation in multiphase size granular mixture geo-disasters. What is more, some scholars (Ng et al. 2017) have proved that some numerical methods such as depth-averaged continuum models are not suitable for investigations of disaster-structure interaction.

For these reasons, the DEM method is used to simulate a series of scenarios in which different configurations of barriers and baffles are made. Input parameters are calibrated by physical tests and numerical experiments. A practical-scale experimental model is built to simulate the practical rock avalanche for exploring effects of barrier configure on capabilities of energy dissipation.

DEM verification

For the investigation of gravity-driven granular materials flowing down an incline slope with DEM modeling, the parameters in models need to be identified first by comparing the numerical results with some bench mark experiments. Accordingly, the lab-scale model tests are introduced for DEM verification.

Rolling resistance linear model

The numerical calculations were performed using the commercial software PFC3D (particle flow code in three dimensions), a simulation tool based on the distinct element method for modeling the dynamic motion and interaction of assemblies of arbitrarily sized spherical particles. The discrete elements, so-called balls, interact with each other by the force-displacement law and Newton's second law of motion (Cundall and Strack 1979).

In this study, a Rolling Resistance Linear Model is applied to model the contact behavior of solid particles. It is based on the linear model, to which a rolling resistance mechanism is added. It can be installed at both ball-ball and ball-facet contacts. The effect of rolling resistance at contacts between particles, and associated energy dissipation, may be of major importance to many granular applications in dense, quasistatic,

and dynamic regimes (Huang et al. 2014, O'Sullivan 2011, Ai et al. 2011). Rolling resistance has been proved as the crucial rule in granular mechanics by several researchers (Oda et al. 1997; Iwashita and Oda 2000). Iwashita and Oda (1998) have done series of numerical studies about shear band experiment using rolling resistance at contacts. The developments of shear bands were simulated well in their researches when the rolling resistance is considered in the DEM. In real granular systems, these mechanisms may have different micro-mechanical origins, such as adhesion of the contact area, or the steric effect due to surface roughness or non-sphericity about the contact point. The rolling resistance contact model provided in PFC is a simple model, based on the linear model, that incorporates a torque acting on the contacting pieces to counteract rolling motion. It is based on the review paper (Ai et al. 2011) and on the work presented in (Wensrich and Katterfeld 2012).

The force-displacement law for the rolling resistance linear model updates the contact force and moment as follows (Itasca 2016):

$$F_c = F^l + F^d, \quad M_c = M^T \tag{1}$$

where F^l is the linear force, F^d is the dashpot force, and M^T is the rolling resistance moment. The linear and dashpot forces are confirmed as in the linear model, while the rolling resistance moment is updated with the bellowing steps.

The rolling resistance moment is incremented as follows:

$$M^T := M^T - k_r \Delta\theta_b \tag{2}$$

where $\Delta\theta_b$ is the relative bend-rotation increment; the rolling resistance stiffness k_r can be defined as follows:

$$k_r = k_s \bar{R}^2 \tag{3}$$

where the $\bar{R}$ is the contact effective radius and can be defined as follows:

$$\frac{1}{\bar{R}} = \frac{1}{R^{(1)}} + \frac{1}{R^{(2)}} \tag{4}$$

As showed in Fig. 1, the $R^{(1)}$ and $R^{(2)}$ are the radii of end (1) and end (2) of the contact respectively. The $R^{(2)}$ will equal to ∞ in the situation of ball-facet contacts.

The rolling resistance linear model provides two additional energy partitions: (1) rolling strain energy, E_{k_r}, stored in the linear spring and (2) rolling slip energy, E_{μ_r}, defined as the total energy dissipated by rolling slip. The whole energy partitions in Rolling Resistance Linear Model are summarized in Table 1.

The rolling strain energy and rolling slip energy can be calculated as follows, respectively:
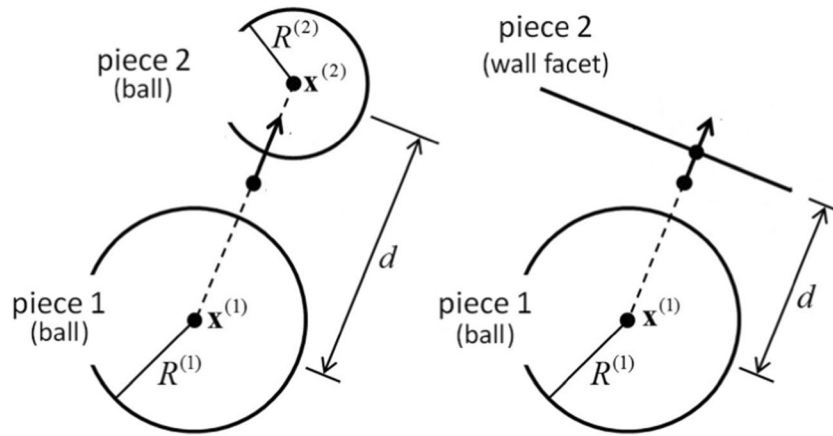
Fig. 1 The contact plane location for the two fundamental contact types: ball-ball and ball-wall

$$E_{\mu r} = \frac{1}{2} \frac{\left\| M^T \right\|^2}{k_r} \qquad (5)$$

$$E_{kr} = E_{\mu r} - \frac{1}{2}\left(\left(M^T\right)_o + M^T\right)\cdot\Delta\theta_b^{\mu r} \qquad (6)$$

The $\Delta\theta_b^{\mu r}$ can be defined as follows:

$$\Delta\theta_b^{\mu r} = \Delta\theta_b - \Delta\theta_b^k = \Delta\theta_b - \left(\frac{M^T - \left(M^T\right)_o}{k_r}\right) \qquad (7)$$

where the $(M^T)_o$ is the rolling resistance moment at the beginning of the time step. The adjusted relative bend-rotation increment of Eq. (2) has been decomposed into elastic $\Delta\theta_b^k$ and a slip $\Delta\theta_b^{\mu r}$ component.

The key parameters' analysis in simulation

The final deposition is a key factor to assess the hazard's risk. In practical engineering, deposition is directly used as an assessment index to analyze the geo-disaster (e.g., landslide, debris flow, and rock avalanches). From the broadest level, deposition includes the runout and the buried depth of geo-disaster. The main parameters that affect the final deposition are different kinds of friction coefficient. There are two kinds of friction coefficient in Rolling Resistance Linear Model: friction coefficient in linear group μ, rolling friction coefficient μ_r in rolling resistance group. To make sure the main influence factor of these two friction coefficient in the simulation of hazard deposition, several experiments are conducted.

The experimental device displayed in Fig. 2 consists of a 0.08-m height cylinder of inner radius R_i resting on a horizontal PVC (Polyvinyl chloride) plane. The tube is partially filled with a volume V_o of mixture glass beads so as to form a column. To make sure the reproducible initial conditions, the tube should always be filled following the same procedure: the glass beads are poured via a funnel onto a sieve placed above the tube, resulting in a homogeneous downfall of grains. The experimental procedure simply consists in quickly removing the tube by means of a lifting system made of rope and pulleys. After it is released, the granular column spreads on the horizontal plane until it comes to rest and forms a deposit. The type of granular material is quartz particle. The mean density is 2.6 g/cm³; mean grain size is 3.0 mm. All particle shapes are standard spheres, all the same size. Subsequent numerical simulations of the models meet the same conditions. Figure 3 (left) shows the experimental setup. Figure 3 (right) shows the side view and top view of granular final deposition.

Several numerical experiments were conducted using the Rolling Resistance Linear Model to confirm the relationship between the final deposition and those two kinds of friction coefficient. Figure 3 shows the experiments in PFC3D. Figure 3a shows the numerical model. The size of this experimental setup

Table 1 Rolling Resistance Linear Model Energy Partitions

Model group	Symbol	Description
Linear group	E_μ	Total energy dissipated by slip
	E_k	Strain energy
Dashpot group	E_β	Total energy dissipated by dashpots
Rolling resistance group	$E_{\mu r}$	Total energy dissipated by rolling slip
	E_{kr}	Rolling strain energy
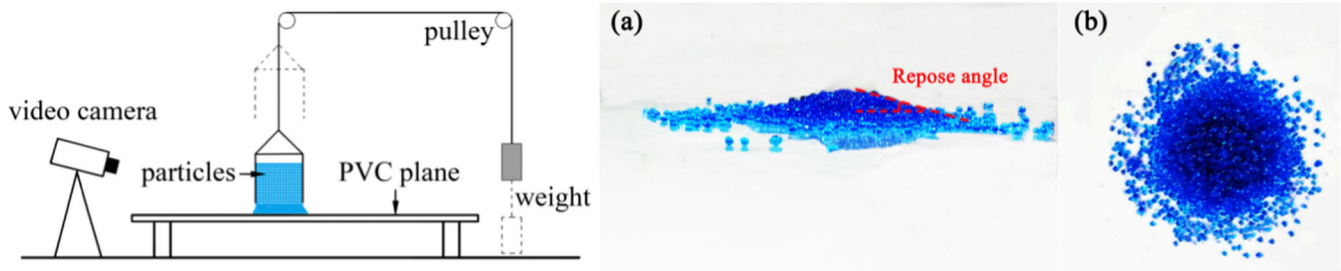
Fig. 2 Laboratory experiment. (left: scheme of the experimental setup; right: **a** side view of final deposition; **b** top view of final deposition)

is as same as the previous studies in Fig. 2. Figure 3b shows the final deposition when $\mu = 0.6$, $\mu_r = 0.2$, whereas Fig. 3c is in the situation of $\mu = 0.2$, $\mu_r = 0.6$. The results show that the final deposition of Fig. 3c is well accordant with the experimental deposition.

Figure 4 shows the variation of repose angle with the changing of rolling friction coefficient μ_r in the situation about two kinds of friction coefficient μ. The results show that the repose angles are determined by these two factors obviously. What is more, some value of repose angle cannot achieve through single kind of friction coefficient. The proper value is determined by the joint action of those two factors.

Problem description, geometry, and parameters

A laboratory experiment is conducted for subsequent DEM modeling to finalize in parameters for further parametric study. The investigation into the impact forces between baffle configuration and rock avalanche was conducted using the numerical experiment.

Experimental model

Figure 5 shows the flume model developed to investigate rock avalanches interacting with a single baffle. The chute is divided to two parts. Its up-part is set to 46° while the down-part set to 10.5°. The former is 0.35-m wide, 8-m long, and the latter is 0.35-m wide, 4-m long.

The distance between the baffle and the end of chute is 0.3 m. Rock avalanches are contained in the storage container located at the upstream end of the flume, which has a maximum volume of 3 m³. The rock avalanches are retained by a spring-loaded door that is secured and controlled by a magnetic lock. Ten force-conductive sensors are installed around the baffle. Force-conductive sensors are used to estimate the avalanches' impact force.
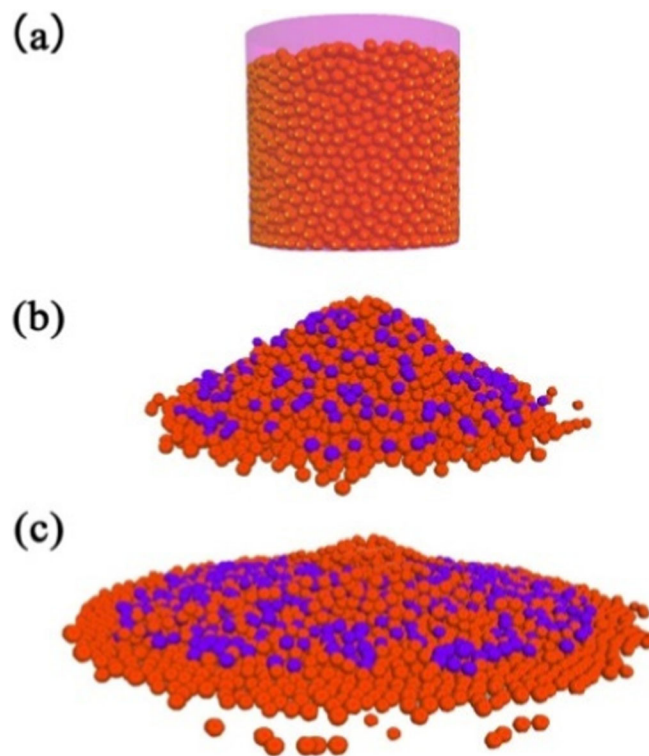
Fig. 3 Numerical experiments in PFC3D. (**a** Initial stage; **b** final deposition with $\mu = 0.6$, $\mu_r = 0.1$; **c** final deposition with $\mu = 0.1$, $\mu_r = 0.6$)
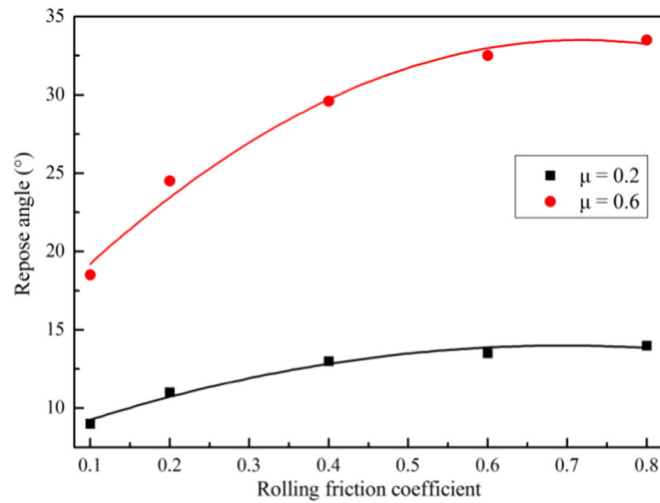
Fig. 4 Variation of repose angle vs. rolling friction coefficient, for different friction coefficient μ

To gain clear insights into the complex fundamental flow mechanism, it is imperative to explore the simplest flow cases first by using dry granular materials. For that end, dry quartz-chips having 6-mm mean diameter are utilized in this study. The quartz-chips material here is the same as in the above experiment. The impact forces are captured by nine force sensors, which are installed at the bottom of obstacle and fixed at the deposition plane. With these nine force sensors installed, it can be ensured that the impact force vector from different directions can be measured. These impact force sensors convert the impact force signal produced by granular flow into an electrical signal based on the resistance-strain effect. The impact area of each force sensor is circular with an area of $\pi \times 0.03^2$ m^2; they collectively cover a total impact area of 0.0254 m^2. The sensors have a measurement range of 0~300 kPa, with a resolution of 0.05 kPa. The radius of force sensor is 0.03 m. The main instruments are shown in Table 2.

Validation of DEM simulation using experimental data

Three major limitations exist in the DEM analysis: (i) particle size is approximated, (ii) only spherical particles are used, and (iii) input parameters are difficult to determine systematically. Although the DEM allows the fundamental particle motions of bouncing, falling, sliding, and rolling to be modeled, some input parameters pertaining to these motions are difficult to determine and quantify accurately and reliably to ensure that input parameters and modeling techniques are appropriate for simulating the interaction of flow against avalanche baffles.

To determine the parameters used in the simulation experiment, two major similitudes are needed for modeling the avalanche-structure interaction: deposition similarity and impact similarity. Deposition similarity is achieved by the comparison of the deposition shape between the physical experiment and the
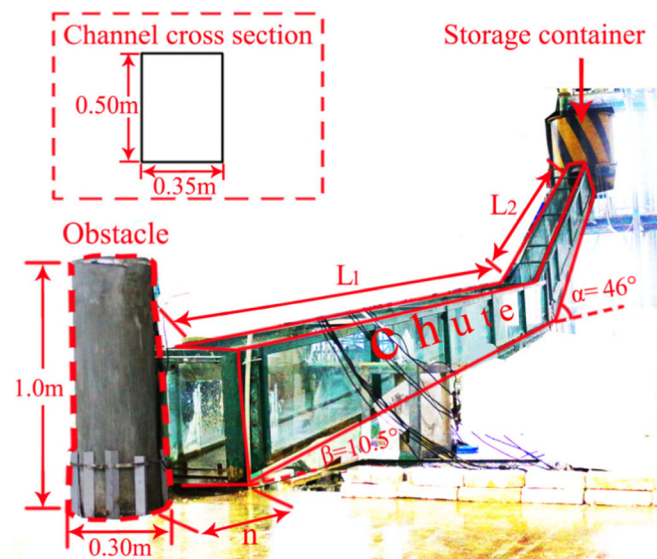
Fig. 5 Flume model used to investigate rock avalanches interacting with a single baffle

Table 2 Instruments list in the laboratory experiments

Instruments	Brand	Model	Parameters	Pictures
Impact force sensors	DHC	JF-YL-30-0.2	Range 300 kPa, ±0.05 kPa	
Data acquisition instrument	DHC	DH5902	16 data channels; Input voltage: ±10 V, ±500 mV	
High speed photography	SVSI	Gigaview	Maximum resolution: 1280×1024; shutter speed: $2×10^{-3}$ ms–30 ms; Spectral range: 400 nm–1000 nm	
PIV	TSI	PIV-1.25	Sampling frequency: >100 Hz	

DEM simulation at different time steps. Impact similarity refers to the comparison of the impact force between or among experiments.

Figure 6 shows the comparison of the instantaneous deposition between the physical experiment and computer simulation at different time steps. At $t = 1.02$ s, the instantaneous deposition of avalanches in laboratory experiments looks like an approximately isosceles triangle; from $t = 6.42$ s, it becomes a butterfly-shape. What is more, the computed analysis shows the same process of shape-change from $t = 1.20$ s to $t = 9.12$ s.

As illustrated in Fig. 7, the measured data in each point is higher than the calculated data. When the distance from obstacle to chute terminal is 0 m, the measured data and calculated data are all the peak values. What is more, the maximum impact forces vary with the changing distance between obstacle and chute terminal (distance n in Fig. 5) in both the experiments are showed in this figure. Those of the simulation are higher than those of the laboratory due to the fact that many gaps exist between the force-conductive sensors to capture all the impact forces. However, both the experiments share a similar force changing trend.

Table 3 summarizes the main material parameters identified by the numerical experiments. Figure 6 shows that the deposition results of simulation agree well with the experimental ones. Meanwhile, Fig. 7 shows that the trend of maximum impact force alteration with different obstacle distance corresponds well with experimental test results. Owing to the good match between the numerical and experimental results, these parameters are applied for a further study of granular avalanches.

Parametric study

A comparison between the experimental and the numerical results indicates that the DEM experiment adopted in this study can well simulate the laboratory experiment. The scale of a laboratory experiment is typically small, and some of its elements such as particle size are difficult to control. Therefore, it is advisable to implement a numerical experiment for investigation of the avalanche-structure interaction.
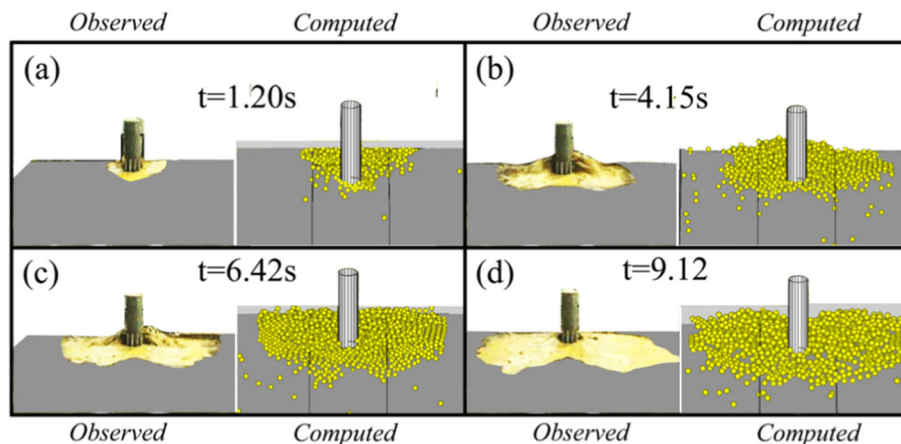
Fig. 6 Flow-obstacle interaction: comparison between laboratory experiment and DEM simulation. **a** Deposition in 1.20 s, **b** deposition in 4.15 s, **c** deposition in 6.42 s, and **d** deposition in 9.12 s
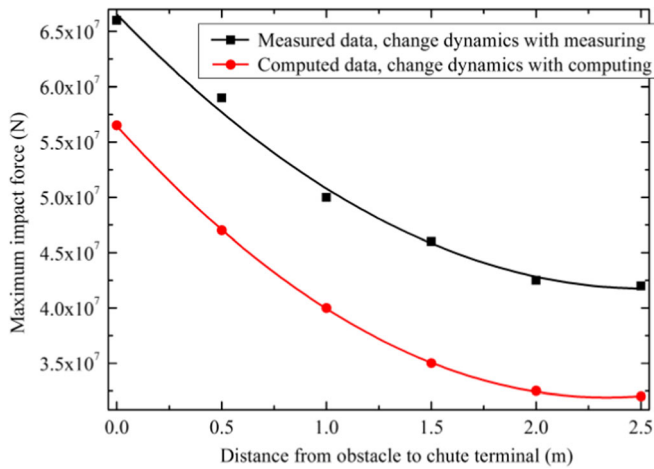
Fig. 7 Maximum impact force comparison between laboratory experiment and DEM simulation

Problem geometry and numerical model

The geometric scheme adopted for this study is shown in Fig. 8, which identifies the key parameters, including the initial avalanche length, width, and height as well as the baffle length, width, height, and spacing. Four rows of baffles are set

Table 3 Material parameters used in the numerical experiments

Name	Value
Normal contact stiffness of ball (MPa/m)	90
Shear contact stiffness of ball (MPa/m)	30
Normal contact stiffness of wall (MPa/m)	90
Shear contact stiffness of wall (MPa/m)	30
Friction coefficient μ	0.20
Rolling resistance coefficient μ_r	0.15
Shear critical damping ratio β_s	0.12
Normal critical damping ratio β_n	0.12

Table 4 Geometrical parameters of slope and defending baffles

| Description	Symbol	Value
Avalanche length [m]	a	36.0
Avalanche width [m]	b	84.0
Avalanche depth [m]	c	6.0
Slope angle 1 [°]	α	50.0
Slope angle 2 [°]	β	20.0
Slope length 1 [m]	L1	60.0
Slope length 2 [m]	L2	54.0
Slope length 3 [m]	L3	200.0
Horizontal baffle length [m]	$l = w$	6.0
Vertical baffle length [m]	h	6.0
Baffle spacing in x direction [m]	n_c	6, 9, 12
Baffle spacing in y direction [m]	n_r	6, 18, 30
Baffle spacing in vertical direction (accurated to one decimal place) [m]	n_v	2.1, 6.2, 10.3
Baffle spacing in horizontal direction (accurated to one decimal place) [m]	n_h	5.6, 16.9, 28.2

and labeled as R1–R4. The slope angle and the relative length of each region are designated using the variables α, β, L_1, L_2, and L_3, respectively. The slope angle is defined relative to the horizontal. In Table 4, numerical values are assigned to all geometric parameters used here. Some researchers have listed relevant data of baffle size (Mast et al. 2014) in practical engineering designing: baffle length, baffle height, and baffle spacing. The baffles here are composed of wall element in PFC3D, which is not breakable after impact. In this study, we only discuss the relationship between energy dissipation and baffle configuration.
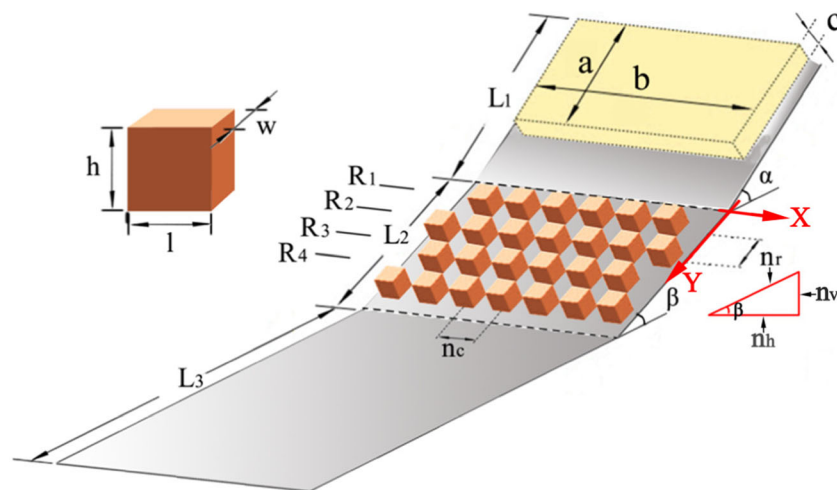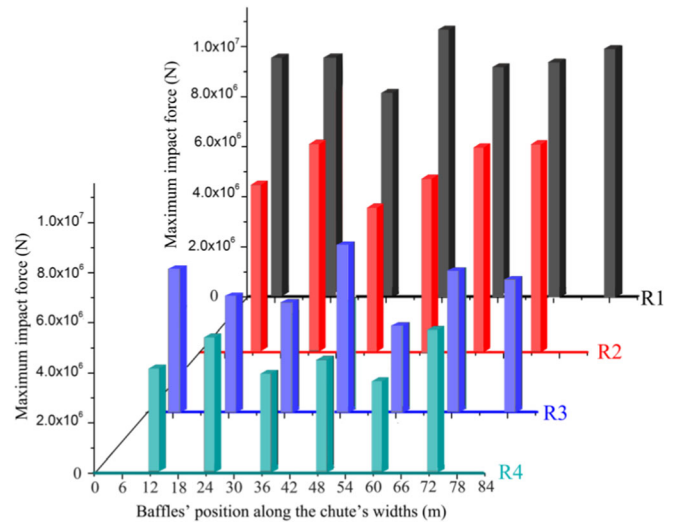

Fig. 8 Geometry of idealized slope
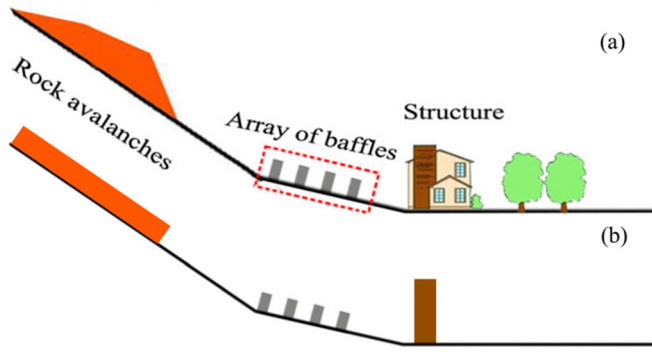
Fig. 9 "Avalanches-baffles-structure" model. **a** Model of practical engineering. **b** Simplified model

Fig. 10 Maximum impact force exerted on single baffle

The slope surface and the defending structure are both represented by "wall elements" (an element type embedded in the PFC3D) in the DEM model. The "wall elements" are characterized by the Coulomb friction law. The wall friction for the ground surface and storage area is set equal to the interparticle friction angle.

The material parameters of the model are the same as those of the comparison model described in the previous section. Materials and particle size of the quartz-chips models here meet the same conditions of the above experiments. Modifications of geometric parameters are made based on the properties of granular avalanches to realize agreement between the experiment and the practical considerations. The main parameters are presented in Table 3, while the changed ones are given in Table 4.

Results

Figure 9 shows the schematic of "avalanches-baffles-structure" model. The building damage caused by rock avalanches is a dynamic process that can be regarded as the combined effect of the rock avalanche's impact, array of baffles' energy dissipation, and structure's response. The array of baffles is usually set up before the building structures. Rock avalanche's kinetic energy

consumption will increase when passing through the baffles. The impact force exerted on the structure reflects the capacity of energy dissipation of an array configuration. For the simplified model, the rectangularly shaped debris flow material may not have the same impact energy compared with the actual case; however, this paper aimed to study the regular variation of impact energy for qualitative analysis rather than quantitative examination. Simplifying the model makes the analysis simpler and easier.

There is no doubt that the impact force exerted on structure is the crucial index that reflects the destructivity of disasters. As the impact force exerted on the building model is a key aspect of avalanche risk analysis, a battery of parametric studies were conducted to unveil the regulars between the impact force and some main parameters such as row distance, column distance, and the number of baffle rows. In the practical engineering, adjusting these three parameters is usually considered as a feasible way to improve the defending-system's energy

Table 5 The main parameters used in the parametric studies to study the impact force exerted from rock avalanches

Case number	Row distance (m)	Column distance (m)	Baffle row's number	Corresponding figure
1	6	6	1, 2, 3, 4	Figure 14
2	6	9	1, 2, 3, 4	
3	6	12	1, 2, 3, 4	
4	6	6, 7, 8, 9, 10, 11, 12	2	Figure 16
5	18	6, 7, 8, 9, 10, 11, 12	2	
6	30	6, 7, 8, 9, 10, 11, 12	2	
7	6	6, 7, 8, 9, 10, 11, 12	3	(with case 4)
8	6	6, 7, 8, 9, 10, 11, 12	4	
9	6, 12, 18, 24, 30	6	2	Figure 19
10	6, 12, 18, 24, 30	9	2	
11	6, 12, 18, 24, 30	12	2	
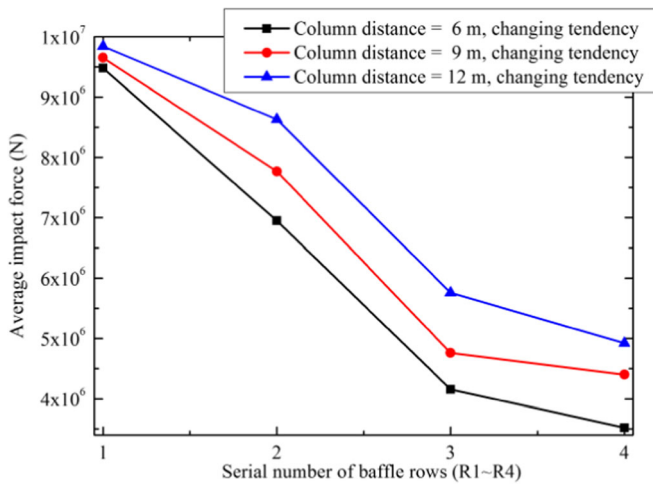
Fig. 11 Average impact force exerted on each baffle row with different column distance

Fig. 13 Impact forces exerted on structure with different baffle rows and calculation step number

dissipation. For this reason, the following studies focus on these main parameters. The variation of the main parameters is summarized in Table 5.

The impact force exerted on the baffles is known to be crucial. In addition, the lower impact force is anticipated to exert on it in the practical engineering. Figure 10 demonstrates the maximum impact force exerted on every single baffle after the rock avalanches passing through these baffles when these horizontal baffle spacing is 6 m. The maximum impact force exerted on R_1 is higher than on the following rows. Figure 11 shows the average impact force exerted on every baffle of each row with different horizontal baffle spacing. The average impact force here means the average impact force from each baffle in every column. Impact force of each baffle is recorded and averaged in every column respectively. Obviously, the nearly linear change is observable in baffle column distance. As the horizontal baffle spacing is reduced, the average impact force exerted on baffles gets smaller.

Influence of baffle row numbers

Figure 12 shows that the energy dissipation in rock avalanches varies with different numbers of baffle rows, with the conspicuous indication that increasing baffle rows does enhance the capacity of particle blocking.

Figure 13 illustrates the impact force evolution with structure change when different row numbers are applied. The rate of force increment rises with the decline of row numbers. Figure 14 gives a glimpse of relationship between maximum impact force and number of baffle rows. The rate of increment about maximum force ascends as the column spacing declines.

Fig. 12 Avalanches' runout comparison (**a–d** rock avalanches flow through different numbers of baffle rows: 4, 3, 2, and 1; **e** rock avalanches flow without baffles)
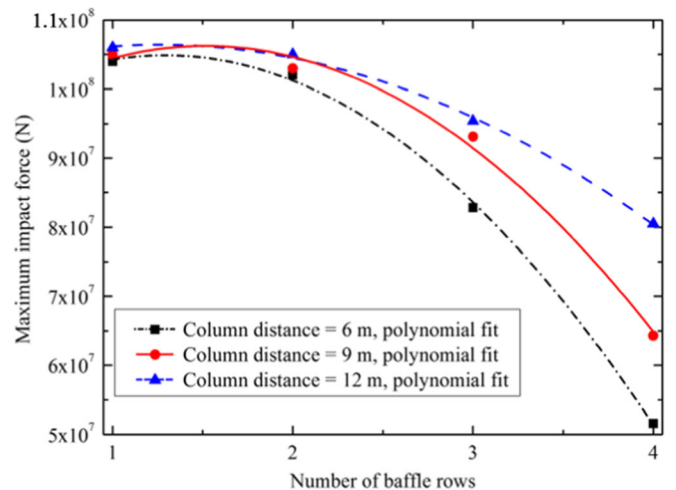

Fig. 14 Maximum impact forces exerted on structure with different column distance and numbers of baffle rows

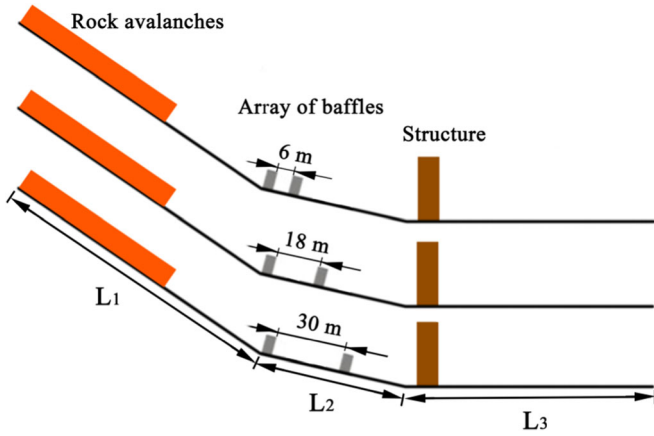**Fig. 15** Changing distance of baffle columns with only two baffle rows

Fig. 17 Maximum impact force exerted on structure with different baffle row numbers and distance of baffle columns

Influence of baffle column spacing

Figure 16 shows that the maximum impact forces exerted on structure varies with the changing distance of baffle columns. Maximum impact force increases as the column spacing increases. What is more, the slope of line increases with the row distance increases. Only two baffle rows (Figs. 15 and 16) are set before the building structure because higher numbers of baffle rows affect the maximum impact force dramatically (Fig. 17). Figure 17 illustrates the relationship between the baffle column spacing and the maximum impact force exerted on structure. The interaction is apparent: the maximum impact force goes up as the column spacing grows larger. This is because the narrow column spacing enables the baffles to retain more particles, thus raising the impact probability between disasters and baffles.

To explain this phenomenon, the images of velocities distribution that avalanches passing through the baffles vary with different distance of baffle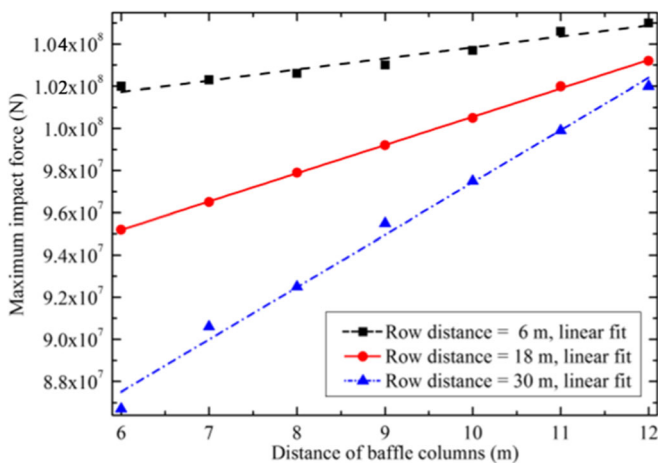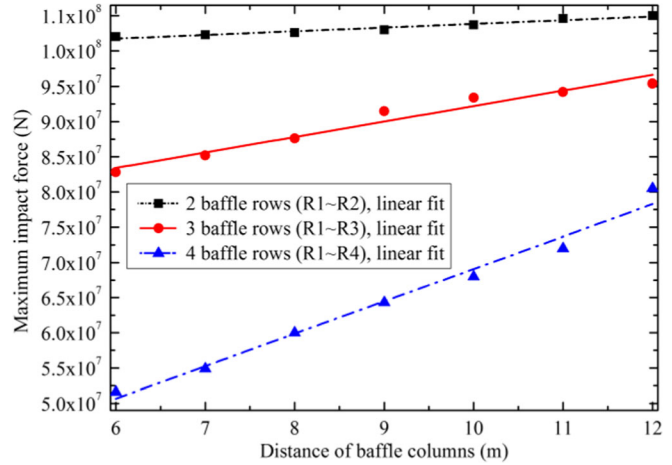 column were made which is showed in Fig. 18. Figure 18(A3) shows that the granular velocities mainly distribute between the values 0.75 and 1 m/s. However, Fig. 18(B3) and (C3) shows that the velocities mainly distributed between the values 1.0 and 1.5 m/s. What is more, the area of value 1.5 m/s in Fig. 18(C3) is much larger than that of Fig. 18(B3).

Figure 18 also shows different avalanches deposition varies with different time steps. Figure 18(A1) shows that when $t =$ 1.82 s, the avalanches deposition has the nearly same shape comparing with Fig. 18(B1) and (C1). The flow regime comparisons of these three situations show that it will take more time steps for the situation of column distance 6 m that avalanches reach the same deposition results comparing to the situation column distance 9 and 12 m. It can be concluded from Fig. 16 obviously that reduce column spacing can decrease the avalanches flow velocities effectively.

Influence of baffle row spacing

Besides, the dense baffles configuration is known to be of strong capability for disaster's energy dissipation. As demonstrated by Fig. 19, at the column distance of 6 m, the maximum impact force exerted on structure is much greater than that at 9 or 12 m. However, the figure also indicates that the maximum impact force declines as the row spacing increases.

The presented result verifies that the row spacing is one of the vital factors that affect the energy dissipation greatly. Besides the effect of baffles, there also exist three other main channels of energy dissipation upon avalanche movement: (1) collision between different particles, (2) friction between particles and slope surface, and (3) friction between different particles. Increasing the row spacing will amplify the effects of the above three. What is more, the increment rate of energy dissipation will rise as the column distance shortens.

To study how the avalanches kinetic changes in more details, the velocity nephogram in Fig. 20 is made to observe the changes when avalanches passing through the baffles. Figure 20(A3) shows that there are small amount of rock fragments between two baffle rows in the time steps of 6.02 s. However, in the same time steps, there are still a number of
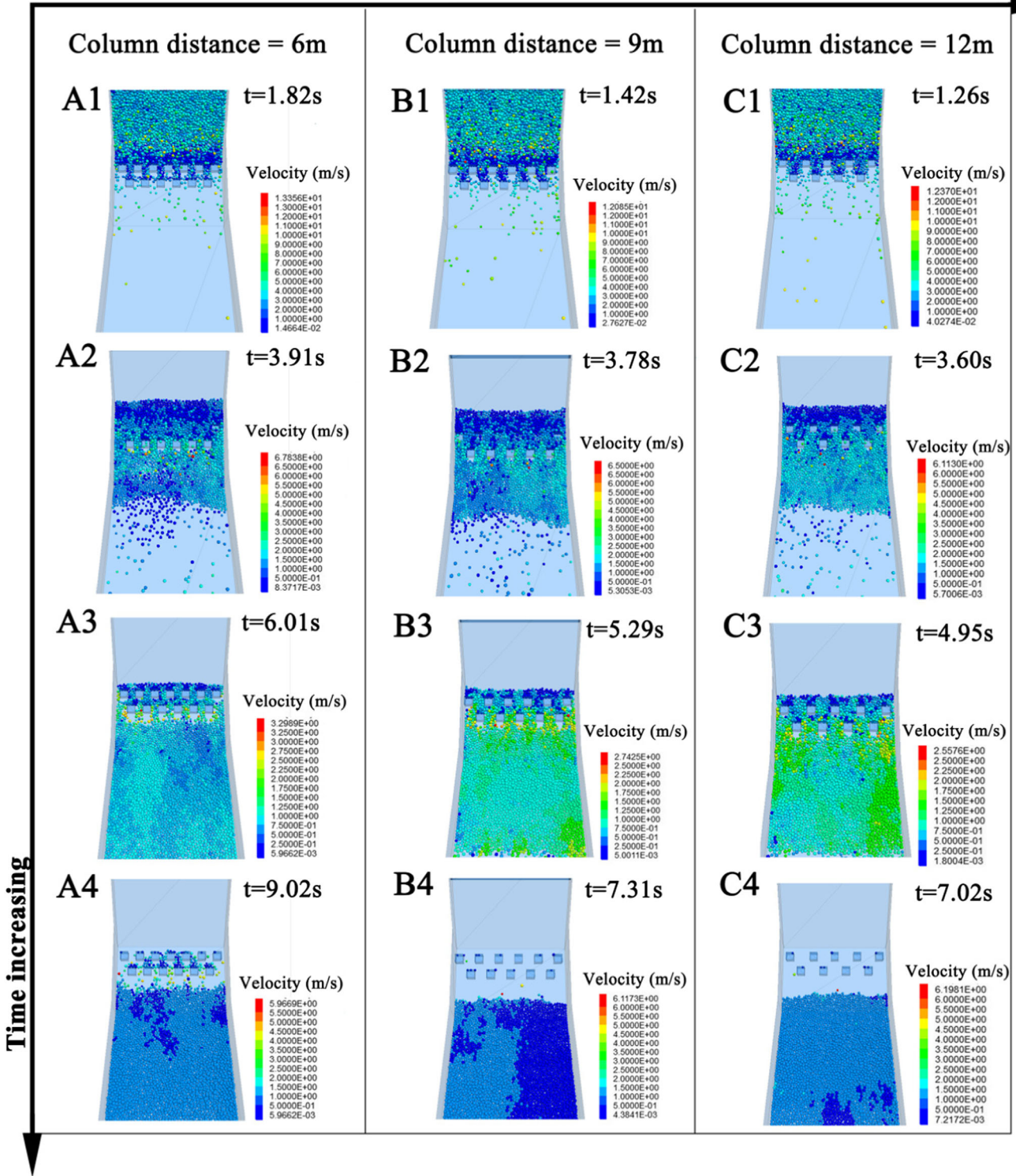

Fig. 16 Maximum impact forces exerted on structure with different distance of baffle columns and row spacing

Fig. 18 Simulated rock avalanches for velocities change under different column distance conditions. (A1–A4) column distance is 6 m, (B1–B4) column distance is 9 m, and (C1–C4) column distance is 12 m
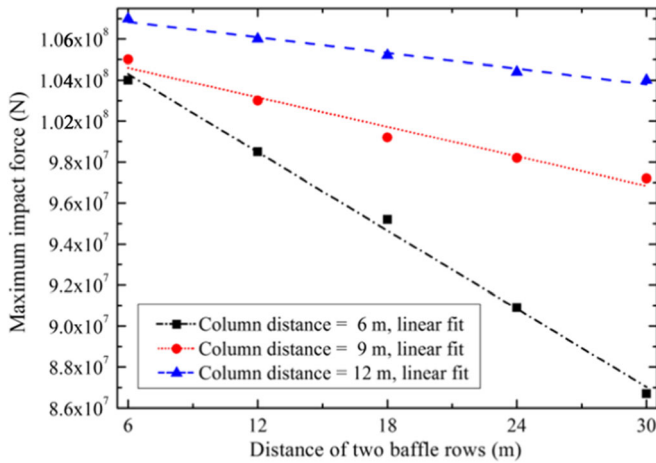
Fig. 19 Maximum impact forces exerted on structure with different distance of baffle rows and column spacing

fragments between two baffles in the situation of row distance 30 m (Fig. 20(C3)). Figure 20(A4) shows that the velocities distribution mainly ranges from 1.0 to 1.5 m/s at the time steps of 9.02 s. Whereas in the Fig. 20(B4), the velocities distribution mainly ranges from 0.5 to 0.75 m/s at the same time steps. What is more, these values mainly range from 0.25 to 0.3 m/s in Fig. 20(C4). As a conclusion, long row distance makes long-lasting effective energy dissipation between avalanches and baffles, which means have more energy dissipation than that of short row distance.

Figure 21 shows the velocities that avalanches passing through those two baffle rows, respectively. Velocities of each rock fragment were recorded and take the average when avalanches crossing baffle gaps. In this study, we make reference to the analyze method of granular flow kinetics which proposed by Savage and Hutter (1989). This method considers that the common expression form of granular flow kinetics can transform into non-dimensional expression form. Thus, despite the size effect in the source area, granular flow in different scales can make the comparison through the non-dimensional expression. The dimensionless forms of travel time and travel velocity can be written as follows:

$$t^* = \frac{t}{\sqrt{L_o/g}} \tag{8}$$

$$U^* = \frac{U}{\sqrt{gL_o}} \tag{9}$$

where t^* is the non-dimensional travel time, t is the normal form of travel time, U^* is the dimensionless form of travel velocity, U is the normal form of travel velocity, g is the gravitational acceleration, and L_o is the length of granular.

Figure 21a shows that the value of solid line is much higher than that of dotted line, while the gap between two lines is decreased along the row distance increased (Fig. 21b). When the row distance equals 30 m (Fig. 21c), these two lines are nearly coincided with each other. This is because that the long row distance makes the enough gap between those two baffle rows (Fig. 20c). When the row distance is shorter as seen in Fig. 20(A1), velocities that rock avalanches pass through the baffle gaps are much slower than that in Fig. 20(B1, C1). Rock avalanches can flow through those two rows smoothly (Fig. 20(B1, C1)) when the enough distance between two rows.

Figure 21 also indicated that the slope in (a3) is steeper than (a2) and (a1), which means that velocity decrease rate of (a3) is higher than that of (a2) and (a1). This phenomenon proved that increasing the row distance can make more energy dissipation when avalanches passing through baffles.

Conclusions

A series of preliminary studies and tests on rock avalanche prevention and mitigation has been conducted, focusing on the impact force investigation of baffle configuration on impedance of rock avalanches. Laboratory experiments were made to identify the appropriate parameters for numerical tests. Based on the numerical verification, discrete element analysis on rock avalanches impinging on arrays of baffles was carried out. As impact force is a crucial index for disaster risk analysis and engineering applications, it is introduced as major factor to reveal the laws between rock avalanches and baffles. Certain outcomes were discussed with particular emphasis on the influences of baffle row numbers, baffle column spacing, and baffle row spacing on the impact forces exerted on the building structure with different arrays of baffles. The study has confirmed that all the three factors have apparent effects on the building structure impact. Increasing the baffle row numbers will enhance the capacity of energy dissipation effectively. However, in the case of fixed baffle row numbers, changing the baffle spacing is another effective method to amplify the efficiency of energy dissipation. In addition to the common consensus that raising the baffle density makes high efficiency, the present study verifies that broadening the baffle row spacing reduces the impact force on building structure. This is because—beside the effect of baffles—three other main channels of energy dissipation exist: upon avalanche movement, (1) collision between different particles, (2) friction between particles and slope surface, and (3) friction between different particles. Hence, it is advisable to consider all these factors in the practical engineering design of baffle configuration.
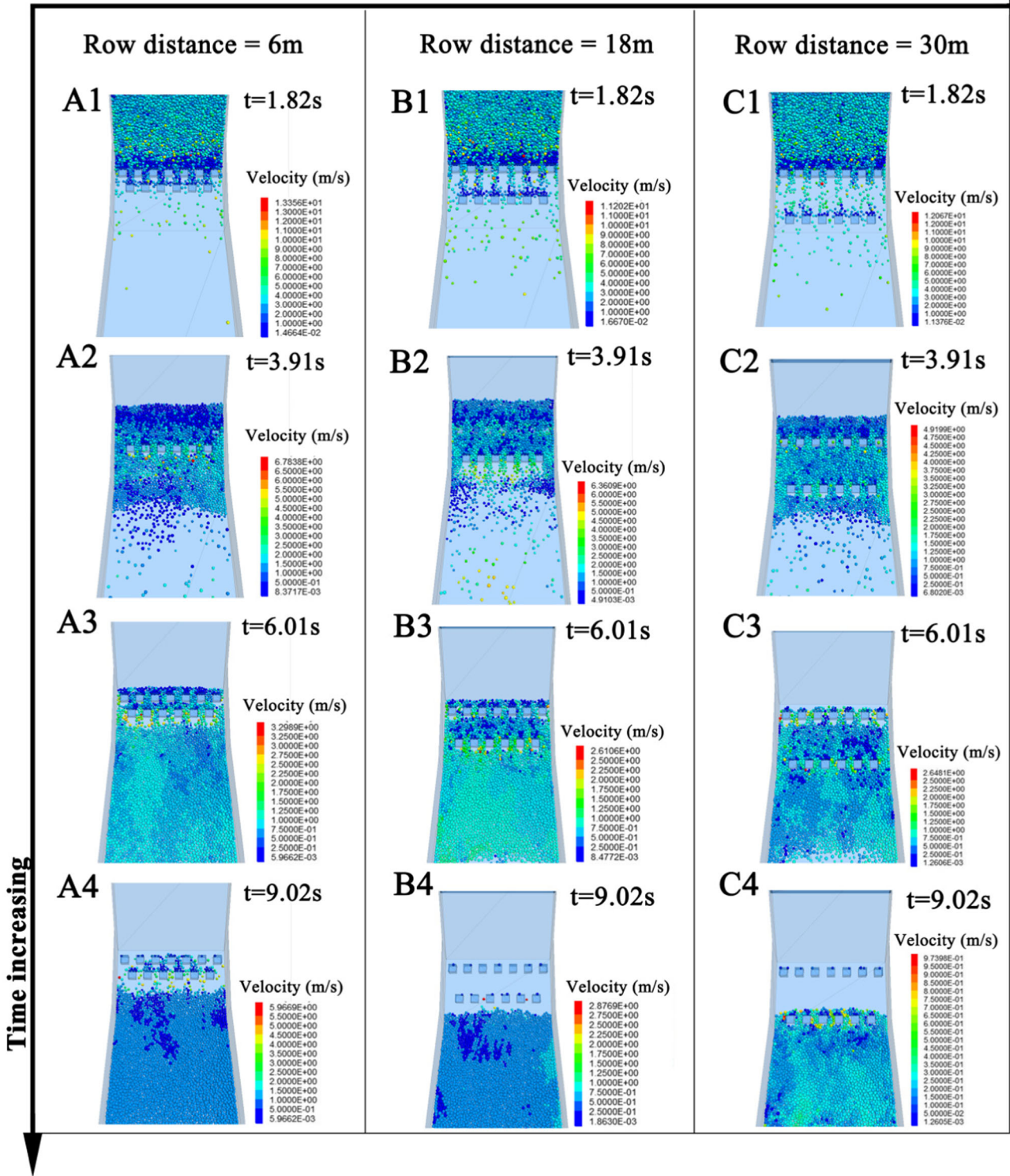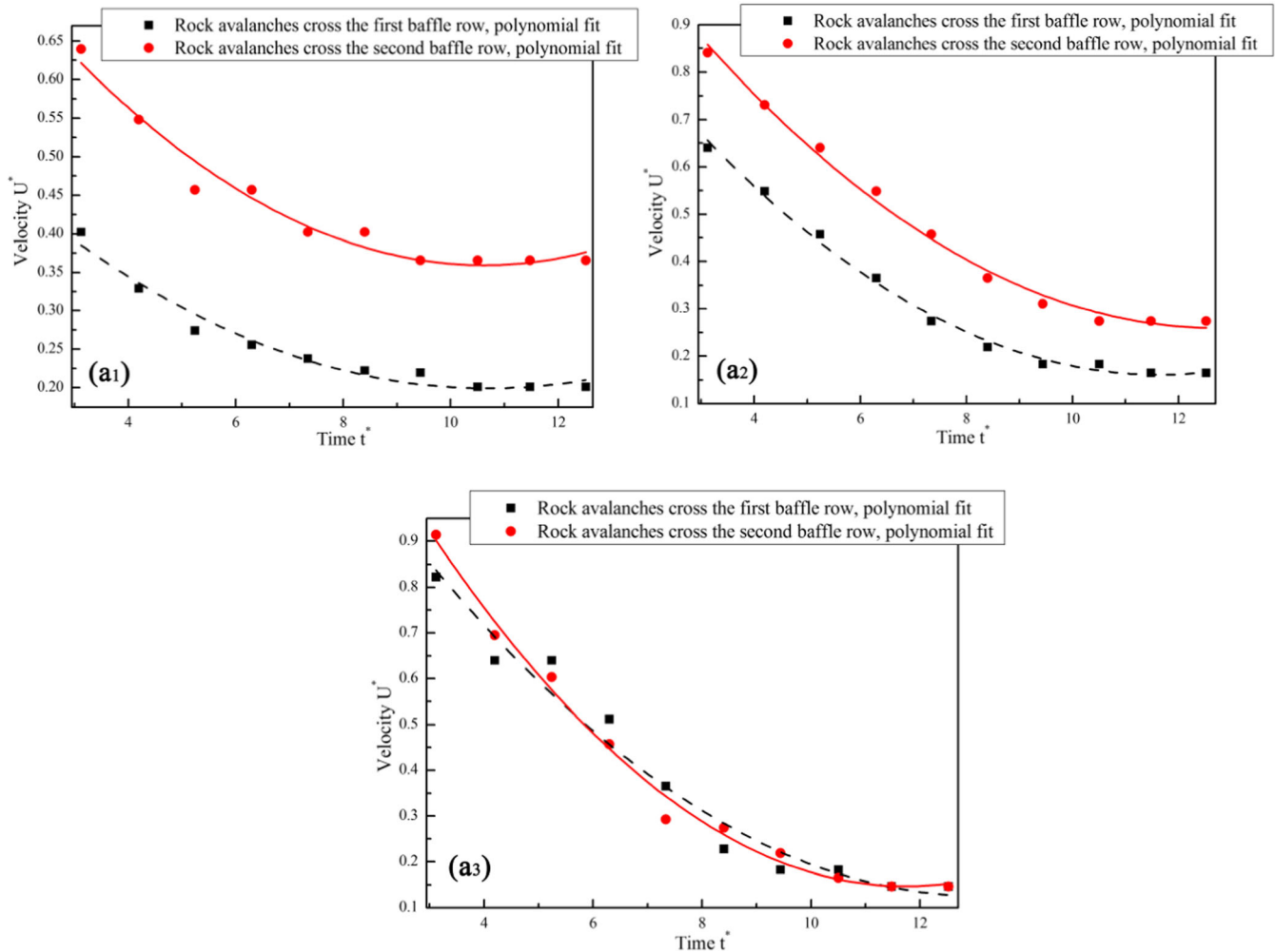
Fig. 20 Simulated rock avalanches for velocities change under different row distance conditions. (A1–A4) row distance is 6 m, (B1–B4) row distance is 18 m, and (C1–C4) row distance is 30 m

Fig. 21 Relationship between velocities that avalanches crossing the baffle rows and time steps with non-dimensional under different row distance conditions. **a1** row distance is 6 m, **a2** row distance is 18 m, and **a3** row distance is 30 m

References

Ai J, Chen JF, Rotter JM, Ooi JY (2011) Assessment of rolling resistance models in discrete element simulations[J]. Powder Technol 206(3):269–282

Bi YZ, He SM, Li XP, Wu Y, Xu Q, Ouyang CJ, Su LJ, Wang H (2016a) Geo-engineered buffer capacity of two-layered absorbing system under the impact of rock avalanches based on Discrete Element Method[J]. J Mt Sci 13(5):917–929

Bi YZ, He SM, Li XP, Ouyang CJ, Wu Y (2016b) Effects of segregation in binary granular mixture avalanches down inclined chutes impinging on defending structures[J]. Environ Earth Sci 75(3):263

Bobrowsky P, Highland L (2013) The landslide handbook-a guide to understanding landslides: a landmark publication for landslide education and preparedness[M]// landslides: global risk preparedness. Springer, Berlin, pp 75–84

Bugnion L, McArdell BW, Bartelt P, Wendeler C (2012) Measurements of hillslope debris flow impact pressure on obstacles[J]. Landslides 9(2):179–187

Calvetti F, di Prisco C, Vairaktaris E (2016) Dry granular flows impacts on rigid obstacles: DEM evaluation of a design formula for the impact force[J]. Proc Eng 158:290–295

Choi CE, Ng CWW, Law RPH et al (2014a) Computational investigation of baffle configuration on impedance of channelized debris flow[J]. Can Geotech J 52(2):182–197

Choi CE, Ng CWW, Song D, Kwan JHS, Shiu HYK, Ho KKS, Koo RCH (2014b) Flume investigation of landslide debris–resisting baffles[J]. Can Geotech J 51(5):540–553

Cruden DM, Novograd S, Pilot GA et al (1990) Suggested nomenclature for landslides[J]. Bull Int Assoc Eng Geol 41(1):13–16

Cundall PA, Strack ODL (1979) A discrete numerical model for granular assemblies[J]. Geotechnique 29(1):47–65

Dai Z, Huang Y, Cheng H, Xu Q (2017) SPH model for fluid–structure interaction and its application to debris flow impact estimation[J]. Landslides 14(3):917–928

de Miranda S, Gentilini C, Gottardi G, Govoni L, Mentani A, Ubertini F (2015) Virtual testing of existing semi-rigid rockfall protection barriers[J]. Eng Struct 85:83–94

Favier P, Bertrand D, Eckert N et al (2012) Optimal design of snow avalanche passive defence structure using reliability approach to quantify buildings vulnerability[C]// EGU General Assembly Conference Abstracts. 14:3–15

Hauksson S, Pagliardi M, Barbolini M, Jóhannesson T (2007) Laboratory measurements of impact forces of supercritical granular flow against mast-like obstacles[J]. Cold Reg Sci Technol 49(1):54–63

Huang X, Hanley KJ, O'Sullivan C, Kwok CY (2014) Exploring the influence of interparticle friction on critical state behaviour using DEM[J]. Int J Numer Anal Methods Geomech 38(12):1276–1297

Hungr O. A (1995) model for the runout analysis of rapid flow slides, debris flows, and avalanches[J]. Can Geotech J 32(4): 610–623.

Hungr O, Leroueil S, Picarelli L (2014) The Varnes classification of landslide types, an update[J]. Landslides 11(2):167–194

Hutchinson JN (2002) Chalk flows from the coastal cliffs of northwest Europe[J]. Rev Eng Geol 15:257–302

Itasca, Consulting Group Inc., 2016. PFC3D particle flow code in 3 dimensions. User's guide. Minneapolis

Iwashita K, Oda M (1998) Rolling resistance at contacts in simulation of shear band development by DEM[J]. J Eng Mech 124(3):285–292.

Iwashita K, Oda M (2000) Micro-deformation mechanism of shear banding process based on modified distinct element method[J]. Powder Technol 109(1):192–205

Jiang YJ, Towhata I (2013) Experimental study of dry granular flow and impact behavior against a rigid retaining wall[J]. Rock Mech Rock Eng 46(4):713–729

Kwan JSH, Koo RCH, Ng CWW (2015) Landslide mobility analysis for design of multiple debris-resisting barriers[J]. Can Geotech J 52(9):1345–1359

Law RPH, Choi CE, Ng CWW (2015) Discrete-element investigation of influence of granular debris flow baffles on rigid barrier impact[J]. Can Geotech J 53(1):179–185

Leonardi A, Wittel FK, Mendoza M, Vetter R, Herrmann HJ (2016) Particle–fluid–structure interaction for debris flow impact on flexible barriers[J]. Comp Aided Civ Inf Eng 31(5):323–333

Li XP, Wu Y, He SM et al (2016) Application of the material point method to simulate the post-failure runout processes of the Wangjiayan landslide[J]. Eng Geol 212:1–9

Liang H, He S, Lei X, et al (2017) Dynamic process simulation of construction solid waste (CSW) landfill landslide based on SPH considering dilatancy effects[J]. Bull Eng Geol Environ 1–15

Mancarella D, Hungr O (2010) Analysis of run-up of granular avalanches against steep, adverse slopes and protective barriers[J]. Can Geotech J 47(8):827–841

Manzella I, Labiouse V (2013) Empirical and analytical analyses of laboratory granular flows to investigate rock avalanche propagation[J]. Landslides 10(1):23–36

Mast CM, Arduino P, Miller GR, Mackenzie-Helnwein P (2014) Avalanche and landslide simulation using the material point method: flow dynamics and force interaction with structures[J]. Comput Geosci 18(5):817–830

Ng CWW, Choi CE, Kwan JSH, Koo RCH, Shiu HYK, Ho KKS (2014) Effects of baffle transverse blockage on landslide debris impedance[J]. Proc Earth Planet Sci 9:3–13

Ng CWW, Choi CE, Song D, Kwan JHS, Koo RCH, Shiu HYK, Ho KKS (2015) Physical modeling of baffles influence on landslide debris mobility[J]. Landslides 12(1):1–18

Ng CWW, Choi CE, Goodwin GR et al (2017) Interaction between dry granular flow and deflectors[J]. Landslides 1–13

O'Sullivan C (2011) Particle-based discrete element modeling: geomechanics perspective[J]. Int J Geomech 11(6):449–464

Oda M, Iwashita K, Kakiuchi T (1997) Importance of particle rotation in the mechanics of granular materials[J]. Powders Grains 97:207–210

Savage S B (1984) The mechanics of rapid granular flows[M]. Advances in applied mechanics. Elsevier, 24:289–366.

Savage SB, Hutter K (1989) The motion of a finite mass of granular material down a rough incline[J]. J Fluid Mech 199:177–215

Spang RM, Rautenstrauch RW (1988) Empirical and mathematical approaches to rockfall protection and their practical applications[C]//5th International Symposium on Landslides. 1237–1243

Tang C, Zhu J, Chang M, Ding J, Qi X (2012) An empirical–statistical model for predicting debris-flow runout zones in the Wenchuan earthquake area[J]. Quat Int 250:63–73

Wensrich CM, Katterfeld A (2012) Rolling friction as a technique for modelling particle shape in DEM[J]. Powder Technol 217:409–417

Xing AG, Xu Q, Gan JJ (2015) On characteristics and dynamic analysis of the Niumian valley rock avalanche triggered by the 2008 Wenchuan earthquake, Sichuan, China[J]. Environ Earth Sci 73(7):3387–3401

Xu Q, Fan XM, Huang RQ, Westen CV (2009) Landslide dams triggered by the Wenchuan Earthquake, Sichuan Province, south west China[J]. Bull Eng Geol Environ 68(3):373–386

Zhan W, Fan X, Huang R, Pei X, Xu Q, Li W (2017) Empirical prediction for travel distance of channelized rock avalanches in the Wenchuan earthquake area[J]. Nat Hazards Earth Syst Sci 17(6):833–844

Zhang Y, Guo C, Lan H, Zhou N, Yao X (2015) Reactivation mechanism of ancient giant landslides in the tectonically active zone: a case study in Southwest China[J]. Environ Earth Sci 74(2):1719–1729

Y. Bi · Y. Du
Institute of Geotechnical Engineering, School of Transportation,
Southeast University,
#.2, Sipailou Road, Nanjing, 210096, China

Y. Bi
e-mail: biyuzhang@seu.edu.cn

S. He · X. Li · H. Liang · Y. Wu
Key laboratory of Mountain Hazards and Earth Surface Process,
Chinese Academy of Science,
Chengdu, 610041, Sichuan, China

S. He
Center for Excellence in Tibetan Plateau Earth Sciences,
Chinese Academy of Sciences,
Beijing, 100101, China

S. He (✉) **· X. Li · H. Liang · Y. Wu**
Institute of Mountain Hazards and Environment (IMHE),
Chinese Academy of Sciences,
#.9, Block 4, Renminnanlu Road, Chengdu, 610041, Sichuan, China
Email: hsm@imde.ac.cn

X. Sun
School of Civil Engineering,
Sichuan University of Science & Engineering,
Zigong, 643000, Sichuan, China

D. Wang
State Key Laboratory of Geohazard Prevention and Geoenvironment Protection,
Chengdu University of Technology,
Chengdu, 610059, Sichuan, China